Exciton Ionization, Franz-Keldysh and Stark Effects in Carbon Nanotubes

Vasili Perebeinos* and Phaedon Avouris

IBM Research Division,

T. J. Watson Research Center,

Yorktown Heights, New York 10598

Nano Letters 2007

(Dated: February 6, 2008)

We calculate the optical properties of carbon nanotubes in an external static electric field directed along the tube axis. We predict strong Franz-Keldysh oscillations in the first and second band-to-band absorption peaks, quadratic Stark effect of the first two excitons, and the field dependence of the bound exciton ionization rate for a wide range of tube chiralities. We find that the phonon assisted mechanism dominates the dissociation rate in electro-optical devices due to the hot optical phonons. We predict a quadratic dependence of the Sommerfeld factor on the electric field and its increase up to 2000% at the critical field of the full exciton dissociation.

Semiconducting carbon nanotubes are direct bandgap materials which have attracted much attention recently for nanophotonic applications [1]. Almost fifty years ago Franz and Keldysh predicted that a static electric field would modify the linear optical properties of the 3D semiconductors near their absorption edge [2, 3]. They showed that the absorption coefficient decays exponentially for photons below the bandgap and shows oscillations for energies above the bandgap. The interest in electroabsorption was revived about three decades latter after discovery of the Quantum-Confined Stark Effect in 2D quantum well structures [4, 5]. Large Stark shifts were observed in fields directed perpendicular to the 2D planes. In 1D carbon nanotubes, excitons were predicted to have large binding energies [6] and to dominate the absorption spectra [7, 8], a fact which was verified experimentally by two-photon spectroscopy [9, 10] and from the observation of the phonon sidebands in photoconductivity spectra [11]. The exciton binding energies in carbon nanotubes have interesting scaling properties [8] and they can be as small as those in 2D structures and as large as 30% of their bandgap depending on both the nanotube structure and the environment.

It has been long recognized that excitonic effects enhance significantly the electroabsorption sig-

nal [12]. An electric field leads to several modifications of the absorption spectrum: 1) modulation of the absorption coefficient; 2) growth of the band-to-band absorption spectral weight; 3) shift of the absorption peak, known as the Stark effect; and 4) dissociation of the bound exciton. In bulk 3D semiconductors the binding energy is small and most of the theoretical and experimental focus has been on the field induced absorption in the region below the bandgap and on the quantum confined Stark effect in 2D structures [13]. In carbon nanotubes, the binding energy is large and the oscillator strength of the higher lying Rydberg states is infinitesimal, so that relatively large changes in the absorption at the first excitonic peak and the first band-to-band absorption are expected.

Here we explore the field induced changes in the absorption spectra of nanotubes for a large range of photon energies as a function of tube chirality and dielectric environment. In opto-electronic carbon nanotube devices, excitons can be produced by electrom-hole recombination or by impact excitation by hot carriers [14, 15, 16]. Therefore, we also address here the problem of the bound exciton dynamics produced in the impact excitation process in an electric field and in the presence of the hot optical phonons. We use a Bethe-Salpeter equation solution for an exciton in the static electric field directed along the tube axis. Similar to Ref. [8] we employ periodic boundary conditions for the unit cell of length L (typically $L \approx 450$ nm) where the electron-hole interaction is computed by including both the direct and exchange Coulomb terms [17]. The nanotube diameter dependence of the exciton binding energies obtained by two-photon fluorescence excitation spectroscopy [18] agrees very well with our model calculations [8] if we choose $\varepsilon = 3.3$, a value that we use in the rest of the paper, unless stated otherwise. The external electric field potential is added to the total Hamiltonian in the Bethe-Salpeter equation. The potential for the relative motion of the exciton has been smoothed out to avoid numerical instabilities:

$$U_F(\vec{r}_e - \vec{r}_h) \;=\; eF\,(z_e - z_h)\tanh\left(k_0\left(\frac{1}{4} - \frac{(z_e - z_h)^2}{L^2}\right)\right) \qquad (1)$$

such that the potential is zero at the unit-cell boundaries at $|z_e - z_h| = \pm L/2$, while at small $|z_e - z_h| \ll L/2$ the hyperbolic tangent equals to unity if we choose the smoothing parameter k_0 to be ≥ 30. The absorption spectra are calculated as in Ref.[8] from the $q = 0$ excitonic wavefunctions.

The absorption spectra at different fields are shown in Fig. 1a. At zero field, there is no absorption in the energy range between the first E_{11} exciton at 0.52 eV and the onset of the first band-to-band (free electron-hole continuum) absorption Δ_{11} at 0.71 eV. The higher energy Rydberg states have

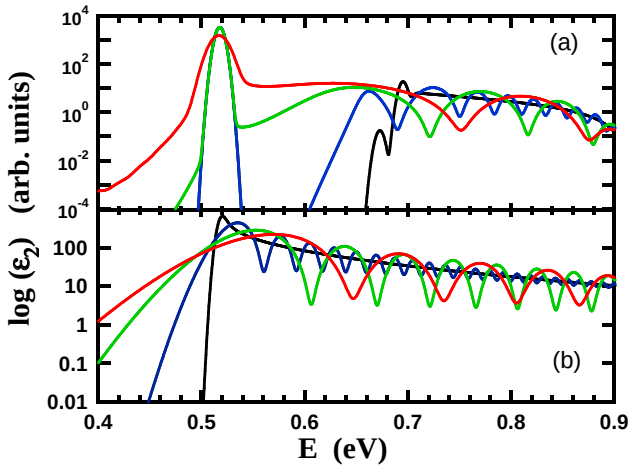

FIG. 1: Absorption spectra in (16, 8) tube d = 1.7 nm in applied electric fields F in V/μm, F = 0.0 (black), 2.0 (blue), 6.0 (green), 10.0 (red) with excitons (a) and for the band-to-band absorption (b) with no excitonic effects. The GW corrections are modeled by the scissor approximation with a scissor value equal to the first exciton binding energy of 194 meV, such that the onsets of zero field spectra in (a) and (b) coincide.

an infinitesimal spectral weight in 1D, except for the highest energy Rydberg state at 0.70 eV, whose energy is in resonance with the onset of the first band-to-band absorption. The interaction between this excitonic state and the band-to-band continuum leads to a spectral weight transfer to the Rydberg exciton, which appears as a peak in the absorption spectra just below the onset of the first band-to-band absorption in Fig. 1a.

At a finite electric field, the band-to-band absorption is modulated and grows in intensity, as shown in Fig. 1a. Similar to the free electron-hole absorption, in the absence of excitonic effects, shown in Fig. 1b, the band-to-band absorption is modulated with a period proportional to the field strength. However, the modifications of the band-to-band absorption in the forbidden region (i. e. below Δ_{11}) in the absence of excitonic effects, and correspondingly the absorption below Δ_{11} and above the excitonic E_{11} peak in the presence of excitons, are very different. In the former case, the free particle absorption decays exponentially in the bandgap region as shown in Fig. 1b, while in the excitonic picture an additional peak develops in the forbidden region, as shown in Fig. 1a. As the field is increased, this peak grows in intensity, moves deeper in the forbidden region, and eventually merges with the E_{11} exciton absorption peak. We define as the exciton dissociation field F_c the field at which the first Franz-Keldysh peak coincides with the E_{11} exciton energy.

At the same time, the "transparent" region between the first two oscillatory peaks broadens and the first absorption minimum moves towards higher energies above the zero-field bandgap edge Δ_{11}. Above the second E_{22} exciton (not shown in Fig. 1a), the second band-to-band absorption above the second bandgap Δ_{22} also shows Franz-Keldysh modulations. However, the absorption coefficient does not go to zero at energies below Δ_{22}, because the first band contributes to the total absorption in that region.

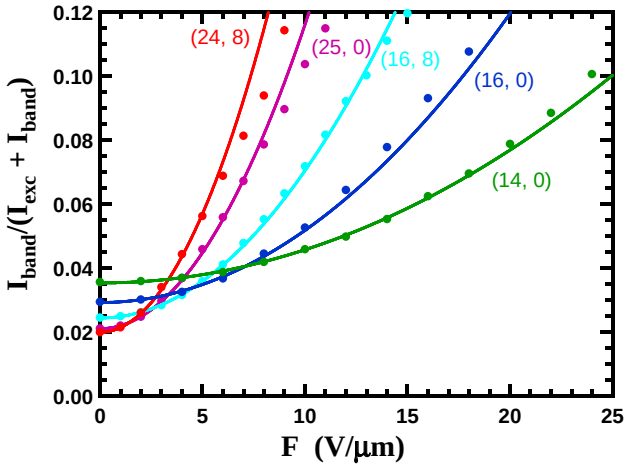

FIG. 2: The relative band-to-band absorption spectral weight as a function of field in (14, 0) tube with $d = 1.1$ nm (green circles), (16, 0) $d = 1.3$ nm (blue circles), (16, 8) $d = 1.7$ nm (cyan circles), (25, 0) $d = 2.0$ nm (magenta circles), and (24, 8) $d = 2.3$ nm (red circles). The solid curves are the best fits to Eq. (2) with $A = 0.009$ and (d_0, κ_s) from table I.

The spectral weight growth of the band-to-band absorption with the electric field is due to the bound exciton wavefunction mixing with the first band-to-band continuum, which leads to spectral weight transfer from the excitonic peak to the latter. As a result, the overall oscillator strength of the first band-to-band absorption grows as much as 400% before the excitonic peak starts to overlap with the tail of the first Franz-Keldysh oscillatory peak. This corresponds to the field strength of about 1/3 of the critical field F_c required for the full exciton dissociation. Upon exciton dissociation the oscillator strength is being transferred to the band-to-band absorption, which is increased from its zero-field value by 10-20 times. The field dependence of the *Sommerfeld factor*, defined here as the fraction of the band-to-band oscillator strength, is shown in Fig. 2 and it can be well fitted by

(n, m)	d	E_b	F_0	d_0	κ_s	κ_b	α
(13, 0)	1.03	281	169	0.026	9.1	4.2	6.3
(14, 0)	1.11	288	198	0.029	7.0	3.0	*9.9*
(12, 4)	1.15	277	179	0.029	7.2	3.2	*7.5*
(16, 0)	1.27	236	119	0.026	7.8	4.0	5.1
(17, 0)	1.35	241	136	0.028	6.4	3.0	5.0
(19, 0)	1.51	204	89	0.025	7.1	3.7	3.5
(20, 0)	1.59	208	99	0.027	6.0	3.1	4.5
(16, 8)	1.68	194	84	0.026	6.1	3.2	4.1
(22, 0)	1.75	179	69	0.025	6.6	*3.6*	3.3
(23, 0)	1.83	182	75	0.026	5.8	3.1	3.9
(25, 0)	1.99	160	54	*0.024*	*6.2*	3.6	3.8
(26, 0)	2.06	162	59	0.025	5.5	*3.1*	3.7
(24, 8)	2.29	142	43	*0.025*	*5.7*	3.5	4.2

TABLE I: Tube indices, diameters in nm, exciton binding energy in meV, and F_0 fields in V/μm in semiconducting carbon nanotubes studied here. The rest of the columns give the best fits for d_0 in nm, κ_s, κ_b, and α in Eq. 2, 3, 4. In italic are shown fit parameters for an averaged fit error larger than 8%. Parameters $A = 0.009$ and $\beta = 1.74$ are kept fixed in the fits.

the following equation:

$$\frac{I_{band}}{I_{band} + I_{exc}} = A + \frac{d_0}{d} + \kappa_s \frac{(edF)^2}{E_b^2} \tag{2}$$

where A, d_0, and κ_s are fit parameters, d is the tube diameter, F is the field strength, e - electron charge, and E_b is the first exciton binding energy. The field dependence in Eq. (2) is motivated by first order perturbation theory for the bound exciton wavefunction mixed by the field with the first band-to-band states separated in energy roughly by the exciton binding energy. The matrix element for the coupling is proportional to the field and the exciton size, which in turn is proportional to the tube diameter [8]. The best fit for all 13 tubes, studied here, is achieved with $A = 0.009$, $d_0 = 0.026$ nm, and $\kappa_s = 6.4$. The exact values used for each individual fit for all 13 tubes are given in table I. In agreement with our predictions the exciton spectral weight reduction has been found to scale quadratically with the applied electric field in recent electroabsorption measurements[19].

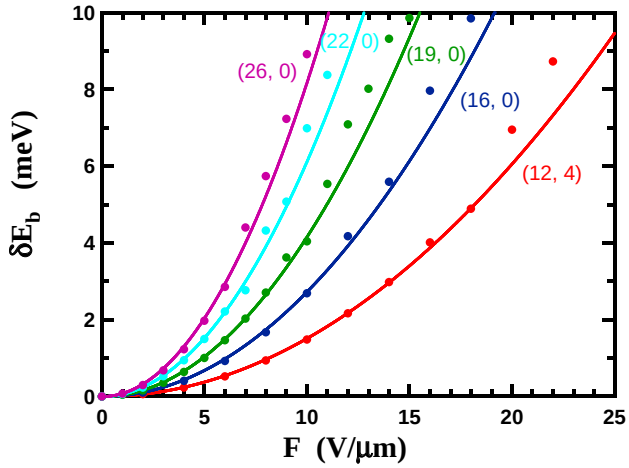

FIG. 3: Exciton binding energy dependence on electric field in (12, 4) tube with $d = 1.15$ nm (red circles), (16, 0) $d = 1.3$ nm (blue circles), (19, 0) $d = 1.5$ nm (green circles), (22, 0) $d = 1.7$ nm (cyan circles), and (26, 0) $d = 2.1$ nm (magenta circles). The solid curves are the best fits to Eq. (2) with κ_b from table I.

The first exciton binding energy increases quadratically with the field, leading to a red-shift of the E_{11} absorption peak. Despite the fact that the first exciton is nearly degenerate with the lower energy dark state [8, 20, 21, 22], we do not find enough mixing between these two states to lead to an observable linear Stark component. The linear Stark effect would be expected only if the off-diagonal coupling strength between the dark and the bright excitons is larger than its energy splitting. In zig-zag tubes the mixing is identically zero and it is negligibly small in chiral tubes. This is due to the different spatial symmetries of these two states, which lead to a negligible dipole moment between them, as was pointed out in Ref [23]. The field dependence of the binding energy is shown in Fig. 3. It is quadratic at low fields, but it deviates from the parabola at higher fields. The quadratic part of the Stark effect can be well described by the following equation:

$$\delta E_b = \kappa_b \frac{(edF)^2}{E_b} \tag{3}$$

whose form is similar to the second order perturbation theory for the bound exciton energy and the exact treatment of the Stark effect in hydrogen atom [24]. A quadratic shift was also observed in the quantum confined Stark effect[4, 25]. The best fit for all 13 tubes studied here is achieved with $\kappa_b = 3.4$. Similar arguments apply to the field dependence of the lower energy dark state. As a result, we find the splitting between the bright and the dark states to be nearly independent of the field strength.

The second E_{22} exciton binding energy has a similar quadratic field dependence suggesting a red shift of the absorption peak, but the magnitude of the shift is typically smaller by a factor of three. The E_{22} exciton can be coupled by the field to states both higher and lower in energy, which would lead to opposite contributions to the sign of the Stark shift. In principle, the sign of the net effect may become reversed, depending on the strength of the couplings to the first and second band states. For $\varepsilon = 3.3$, we find E_{22} to always red-shift (increase of the binding energy) with field, but the net effect is reduced in magnitude. However, when we reduce the dielectric constant to $\varepsilon = 2.0$, the second exciton binding energy increases, the E_{22} resonance comes close to the first band-to-band absorption peak, and the coupling to the latter dominates leading to an overall E_{22} blue shift. At even higher fields of about $F \geq 10$ V/μm and $\varepsilon = 2.0$, we find that the sign of the second exciton Stark shift suddenly reverses and we obtain a red-shift. This nonperturbative result can be explained by the Franz-Keldysh modulation of the band-to-band states.

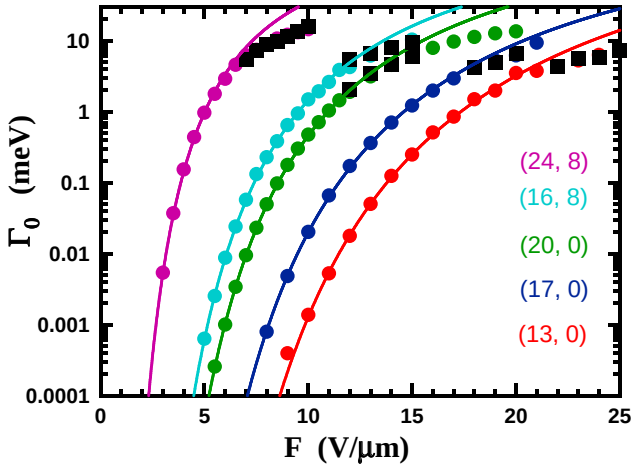

FIG. 4: Exciton dissociation rate as a function of field in (13, 0) tube with $d = 1.0$ nm (red), (17, 0) $d = 1.35$ nm (blue), (20, 0) $d = 1.6$ nm (green), (16, 8) $d = 1.7$ nm (cyan), and (24, 8) $d = 2.3$ nm (magenta). The black squares are the linewidths from the absorption fit to the Fano lineshape. The solid curves are the best fit to Eq. (1) with $\beta = 1.74$ and α from table I.

Under an applied field, a bound exciton can dissociate into a free electron and a hole in the first continuum band, which may contribute, for example, to photoconductivity [26]. The exciton field dissociation rate determines the bound exciton lifetime and results in the broadening of the E_{11} absorption peak. At high fields, we can determine the bound exciton dissociation rate by fitting the E_{11} absorption from the Bethe-Salpeter equation solution to the Fano lineshape. The results of

the fits are shown in Fig. 4 by the black squares. When the broadening becomes less than 1 meV, this procedure can no longer be used. For smaller fields, we determine the lifetime by calculating the tunneling probability of the bound exciton into the free electron-hole continuum, from the leaking of the exciton wavefunction away from the central region. The exciton wavefunctions for different fields are shown in Fig. 5. We calculate the tunneling probability from the wavefunction weight at an electron-hole separation larger than 50 nm[27]. To convert the tunneling probability into the decay rate, we need to know the "attempt" frequency for tunneling. From the Heisenberg uncertainty principle, an averaged momentum of the bound exciton is $p = 2\pi\hbar/\lambda$, where λ is the exciton size. According to the virial theorem, the exciton binding energy E_b is proportional to the kinetic energy $E_k \approx pv/2$, where v is an averaged velocity. In 3D case, $E_b = E_k$, and, therefore, one would expect, in the case of nanotubes, an attempt frequency $v/(2\lambda)$ to scale with $E_b/(2\pi\hbar)$. By adjusting the attempt frequency to agree with the lifetime calculations from the absorption linewidth, we can obtain the bound exciton dissociation rate in a wide range of electric fields shown in Fig. 4. The attempt frequency varies from 1 to 1.5 times $E_b/(2\pi\hbar)$. The exciton dissociation rate can be well-fitted by the following equation:

$$\Gamma_0(F) = \alpha E_b \frac{F_0}{F} \exp\left(-\frac{F_0}{F}\right) \tag{4}$$

where $F_0 = \beta E_b^{3/2} m^{1/2}/e\hbar$, m is a reduced exciton mass ($m^{-1} = m_e^{-1} + m_h^{-1}$). This form is motivated by the solution of the hydrogen atom in an applied electric field [28]. It should be noted here, that the electron and hole dispersions in CNTs are hyperbolic, unlike parabolic dispersion typically used in exciton dissociation description in solids. The best fit for all 13 tubes, studied here, is obtained for $\alpha = 4.1$ and $\beta = 1.74$. As seen from Fig. 4, at high fields $F/F_0 \geq 0.14$, the tunneling rate from Eq. (1) deviates from the numerical result. The criterion for the full exciton dissociation[29] is satisfied at a field strength of $F_c \approx F_0/2$. It is instructive to compare the present results with those obtained for the 2D exciton ionization rates in fields parallel to the quantum well plane. [25]. The exciton ionization in the latter is one order of magnitude smaller due to the difference in exciton mass and binding energy.

It has recently been shown that under high bias the energetic carriers in nanotubes excite optical phonons [30, 31, 32, 33] and generate a non-equilibrium phonon distribution [34, 35], particularly when energy dissipation to the substrate is suppressed as in suspended CNTs [35]. Therefore, one may expect that the produced excitons, for example, in electroluminescence experiments [14], can

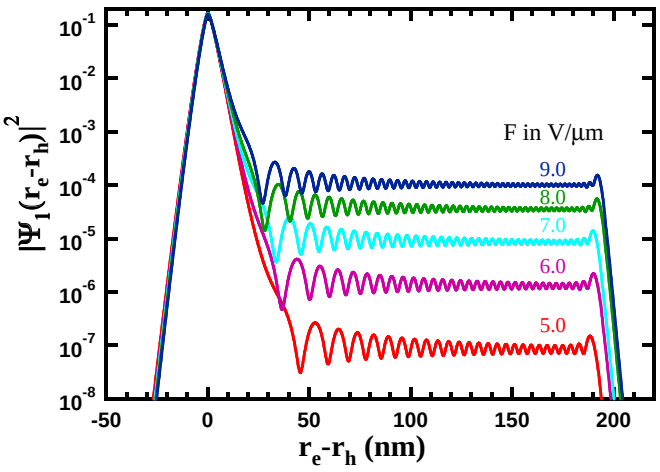

FIG. 5: Optically active exciton wavefunction for different fields $F = 5.0$ (red), 6.0 (magenta), 7.0 (cyan), 8.0 (green), and 9.0 (blue) V/μm. There is a finite probability for exciton to dissociate, which is found from the wavefunction weight outside the central region $|r_e - r_h| \geq 50$ nm.

experience a phonon assisted dissociation. To explore this mechanism, we need to model the energy distribution function of excitons, which is determined by the coupling to the optical phonon bath and the spectral function of the pumping source of excitons. The optical phonon bath is assumed to be at temperature T_{op} and the pumping source of excitons is assumed to be tuned at the E_{11} energy with intensity P_0. The bound exciton with zero momentum can absorb an optical phonon with momentum $-q$ and be promoted to state q with an optical phonon energy $\hbar\omega_{ph}$ above the bottom of the exciton band E_{11}. The probability of this event is proportional to the optical phonon occupation number $n_{ph}(-q)$ and the strength of the exciton-optical phonon coupling. In the reverse process, the high energy q-exciton can emit a phonon and be relaxed to the bottom of the exciton band. This probability is proportional to the product of $(1 + n_{ph}(-q))$ and the strength of the exciton-optical phonon coupling. Since the phonon dispersion is much smaller than the exciton dispersion, we can reduce the problem to the two level system described by the rate equations:

$$\begin{aligned} \frac{\partial N_0}{dt} &= P_0 - N_0\frac{\Gamma_0}{\hbar} - N_0\frac{n_{ph}}{\tau_{ph}} + N_1\frac{1+n_{ph}}{\tau_{ph}} \\ \frac{\partial N_1}{dt} &= -N_1\frac{\Gamma_1}{\hbar} - N_1\frac{1+n_{ph}}{\tau_{ph}} + N_0\frac{n_{ph}}{\tau_{ph}} \end{aligned} \tag{5}$$

where N_0 and N_1 are the ground and vibrationally excited states, n_{ph} is given by the Bose-Einstein factor, and the scattering time $\tau_{ph} \approx 30 - 100$ fs is determined by the exciton-optical phonon coupling strength. The exciton-optical phonon scattering time has been calculated [36] and is of

the same order of magnitude with the measured [30, 31, 32] and calculated [33, 34] electron-optical phonon scattering time. The dissociation rate of the excited state Γ_1 is much faster than that of the ground state Γ_0. It can be modeled by Eq. (4) with binding energy replaced by $E_b - \hbar\omega_{ph}$, where $\hbar\omega_{ph} \simeq 200$ meV is the optical phonon energy. Note that in the absence of the exciton pumping source $P_0 = 0$ and the exciton decay channels $\Gamma_{0,1} = 0$, equation 5 gives a steady state thermal exciton distribution in equilibrium with the optical phonon sink bath. The net exciton dissociation rate, including the phonon assisted mechanism, can be obtained from:

$$\Gamma(T_{op}) = \frac{\Gamma_0 N_0 + \Gamma_1 N_1}{N_0 + N_1} = \frac{\Gamma_0 \left(1 + n_{ph} + \tau_{ph}\Gamma_1/\hbar\right) + \Gamma_1 n_{ph}}{1 + 2n_{ph} + \tau_{ph}\Gamma_1/\hbar} \tag{6}$$

where N_0 and N_1 give the steady state solution in Eq. (5). In the limit of a very efficient thermalization, $\tau_{ph}\Gamma_1 \ll 1$, the exciton ionization rate from Eq. 6 is given by the thermal average of the decay rates of the two states. On the other hand, in the opposite limit $\tau_{ph}\Gamma_1 \gg 1$, which is realized, for example, when the vibrationally excited state is above the band-to-band continuum, $E_b \leq \hbar\omega_{ph}$, the exciton dissociation rate depends also on the exciton-optical phonon scattering time as $\Gamma(T_{op}) \approx \Gamma_0 + n_{ph}/\tau_{ph}$. Even at room temperature, the phonon assisted contribution to the dissociation rate can be appreciable, especially at low fields, due to the strong exciton-optical phonon interaction in carbon nanotubes. In opto-electronic devices operating at high currents, the phonon assisted mechanism would dominate the net exciton dissociation rate due to the high optical phonon occupation.

In conclusion, we predict strong modulation of the absorption spectra of carbon nanotubes by the electric field. We find a large electric field enhancement of the band-to-band absorption, or the Sommerfeld factor, and a large red Stark shift of the bound exciton, especially in large diameter tubes. We find that the bound exciton ionization rate depends strongly on field strength and can be in the sub-picosecond range at moderately high electric fields. Finally, optical phonon occupation, which can be high in opto-electronic devices, dramatically increases exciton dissociation.

---

[*] Electronic address: vperebe@us.ibm.com

[1] Avouris, Ph.; Chen. J. *Materials Today* **2006**, *9*, 46.

[2] Franz, W. *Z. Naturforsch.* **1958**, *13a*, 484.

[3] Keldysh, L. V. *Zh. Eksp. Teor. Fiz.* **1958**, *34*, 1138. [*Sov. Phys.-JETP* **1958**, *7*, 788.]

[4] Miller, D. A. B.; Chemla, D. S.; Damen, T. C.; Gossard, A. C.; Wiegmann, W.; Wood, T. H.; Burrus, C. A. *Phys. Rev. Lett.* **1984**, *53*, 2173.

[5] Miller, D. A. B.; Chemla, Schmitt-Rink, S. *Phys. Rev. B* **1986**, *33*, 6976.

[6] Ando, T, *J. Phys. Soc. Jpn.* **1997**, *66*, 1066.

[7] Spataru, C. D.; Ismail-Beigi, S.; Benedict, L. X.; Louie, S. G. *Phys. Rev. Lett.* **2004**, *92*, 077402.

[8] Perebeinos, V.; Tersoff, J.; Avouris, Ph. *Phys. Rev. Lett.* **2004**, *92*, 257402.

[9] Wang, F.; Dukovic, G.; Brus, L. E.; Heinz, T. F. *Science* **2005**, *308*, 838.

[10] Maultzsch, J.; Pomraenke, R.; Reich, S.; Chang, E.; Prezzi, D.; Ruini, A.; Molinari, E.; Strano, M. S.; Thomsen, C,; Lienau, C. *Phys. Rev. B* **2005**, *72*, 241402R.

[11] Qiu, X.; Freitag, M.; Perebeinos, V.; Avouris, Ph. *Nano Lett.* **2005**, *5*, 749.

[12] See, for example, Dow, J. D.; Redfield, D. *Phys. Rev. B* **1970**, *1*, 3358.

[13] Haug, H.; Koch, S. W. In *Quantum Theory of the Optical and Electronic Properties of Semiconductors* World Scientific: London, 2005.

[14] Chen, J.; Perebeinos, V.; Freitag, M.; Tsang, J.; Fu, Q.; Liu, J.; Avouris, Ph. *Science* **2005**, *310*, 1171.

[15] Marty, L.; Adam, E.; Albert, L.; Doyon, R.; Mnard, D.; Martel, R. *Phys. Rev. Lett.* **2006**, *96*, 136803.

[16] Perebeinos, V.; Avouris, Ph. *Phys. Rev. B* **2006**, *74*, 121410.

[17] Rohlfing, M.; Louie, S. G. *Phys. Rev. B* **2000**, *62*, 4927.

[18] Dukovic, G.; Wang, F.; Song, D.; Sfeir, M. Y.; Heinz, T. F.; Brus, L. E. *Nano Lett.* **2005**, *5*, 2314.

[19] Kennedy, J. W.; Vardeny, Z. V.; Collins, S.; Baughman, R. H.; Zhao, H.; Mazumdar, S. cond-mat/0505071.

[20] Zhao, H.; Mazumdar, S. *Phys. Rev. Lett.* **2004**, *93*, 157402.

[21] Perebeinos, V.; Tersoff, J.; Avouris, Ph. *Nano Lett.* **2005**, *5*, 2495.

[22] Spataru, C. D., Ismail-Beigi, S., Capaz, R. B.; Louie, S. G. *Phys. Rev. Lett.* **2005**, *95*, 247402.

[23] Barros, E. B.; Capaz, R. B.; Jorio, A.; Samsonidze, G. G.; Filho, A. G. S.; Ismail-Beigi, S.; Spataru, C. D.; Louie, S. G.; Dresselhaus, G.; Dresselhaus, M. S. *Phys. Rev. B* **2006**, *73*, 241406R.

[24] Alexander, M. H. *Phys. Rev.* **1969**, *178*, 34.

[25] Miller, D. A. B.; Chemla, D. S.; Damen, T. C.; Gossard, A. C.; Wiegmann, W.; Wood, T. H.; Burrus, C. A. *Phys. Rev. B* **1985**, *32*, 1043.

[26] Mohite, A.; Lin, J.-T.; Sumanasekera, G.; Alphenaar, B. W. *Nano Lett.* **2006**, *6*, 1369.

[27] We find oscillations of the tunneling probability with the size of unit cell L and we choose its value at the minimum.

[28] Bethe, H. A.; Salpeter E. E. in *Quantum mechanics of One- and Two- electron atoms* (Academic, New York **1957**).

[29] Here we use an equivalent definition of the exciton dissociation field F_c, as the field at which the exciton

dissociation rate (linewidth) becomes comparable to the exciton binding energy, i. e. $\Gamma_0(F_c) \approx E_b$.

[30] Yao, Z.; Kane, C. L.; Dekker, C. *Phys. Rev. Lett.* **2000**, *84*, 2941.

[31] Javey, A.; Guo, J.; Paulsson, M.; Wang, Q.; Mann, D.; Lundstrom, M.; Dai, H. *Phys. Rev. Lett.* **2004**, *92*, 106804.

[32] Park, J. Y.; Rosenblatt, S.; Yaish, Y.; Sazonova, V.; Ustunel, H.; Braig, S.; Arias, T. A.; Brouwer, P.; McEuen, P. L. *Nano Lett.* **2004**, *4*, 517.

[33] Perebeinos, V.; Tersoff, J.; Avouris, Ph. *Phys. Rev. Lett.* **2005**, *94*, 086802.

[34] Lazzeri, M.; Piscanec, S.; Mauri, F.; Ferrari, A. C.; Robertson, J. *Phys. Rev. Lett.* **2005** *95*, 236802.

[35] Pop, E.; Mann, D.; Cao, J.; Wang, Q.; Goodson, K.; Dai, H. *Phys. Rev. Lett.* **2005**, *95*, 155505.

[36] Perebeinos, V.; Tersoff, J.; Avouris, Ph. *Phys. Rev. Lett.* **2005**, *94*, 027402.